

Silicon nitride membrane resonators at millikelvin temperatures with quality factors exceeding 10^8

Mingyun Yuan,^{1, a)} Martijn A. Cohen,¹ and Gary A. Steele¹

*Kavli Institute of Nanoscience, Delft University of Technology, PO Box 5046,
2600 GA, Delft, The Netherlands*

(Dated: 5 April 2024)

We study mechanical dissipation of the fundamental mode of millimeter-sized, high quality-factor (Q) metalized silicon nitride membranes at temperatures down to 14 mK using a three-dimensional optomechanical cavity. Below 200 mK, high- Q modes of the membranes show a diverging increase of Q with decreasing temperature, reaching $Q = 1.27 \times 10^8$ at 14 mK, an order of magnitude higher than reported before. The ultra-low dissipation makes the membranes highly attractive for the study of optomechanics in the quantum regime, as well as for other applications of optomechanics such as microwave to optical photon conversion.

^{a)}Electronic mail: m.yuan@tudelft.nl

Mechanical resonators made from silicon nitride have shown great potential for both fundamental research and applications. They have become platforms for studying quantum optomechanics,^{1–10} and key elements for applications such as optical to micro- and radio-wave photon transducers^{11,12} and NEMS/MEMS sensors.^{13–15} High-stress SiN_x devices typically have very high quality factors, which is a key parameter for a mechanical resonator. In optomechanics, low dissipation reduces the mechanical resonator’s coupling to the environment and improves the cooperativity, enabling cooling to a lower temperature and state preparation with higher fidelity. High quality factors also enhance the efficiency of a transducer as well as the sensitivity of a NEMS/MEMS sensor.

Studies of the quality factor of SiN_x resonators have found at room temperature Q of up to 10^6 for nanostrings,¹⁶ 10^5 for beams,^{13,14} 10^5 for trampolines,¹⁷ and 10^6 for the fundamental mode of membranes.¹⁸ Higher modes of membranes have been observed to have higher Q -factors,^{19,20} up to 5×10^7 ,²⁰ but show weaker optomechanical coupling $g_0 = \frac{d\omega_0}{du}u_{zpf}$ (ω_0 , the cavity mode frequency; u , the mechanical displacement and u_{zpf} , the amplitude of the zero-point fluctuation) and have smaller mode spacing leading to a dense mode spectrum. Smaller membranes were previously studied down to millikelvin temperatures, but Q was relatively low due to their lower aspect ratio.²¹ Measurements of the Q of the fundamental mode of millimeter-sized membranes down to 300 mK demonstrated a plateau in Q below 1K at a value up to 10^7 .¹⁸ A recent comprehensive review can be found in Ref. 22.

Here, we study the quality factor of large, high- Q SiN_x membranes at temperatures down to 14 mK. We use a three-dimensional (3D) superconducting optomechanical cavity¹⁰ to detect the motion. Similar to previous reports, we observe a plateau in Q down to 200 mK. Below 200 mK, we observe a new behavior of the quality factors of high- Q modes that diverges down to the lowest temperature we can measure, reaching a record of $Q = 1.27 \times 10^8$ for a fundamental mode at 14 mK, promising for future applications in optomechanics in both the microwave and optical domains.

A photograph of the device is shown in Fig. 1(a). The 3D cavity is formed by two halves of a machined Al block. An SMA connector is partially inserted into the cavity for reflection measurement. The mechanical resonator is a Norcada SiN_x membrane which can be seen on the sapphire support substrate. We present here results from the two membranes we have studied at these temperatures. The membranes are 50 nm thick in a square of size $l \times l$ with $l = 1.5$ mm for Device I and $l = 1$ mm for Device II. Device I is stoichiometric

with $x = 3/4$ and a tensile stress of 0.8 GPa. Device II has a tensile stress of ≤ 0.25 GPa and x is not specified by the manufacturer. We deposit a metal layer of 20 nm of Al on the membrane which forms a capacitor with the antenna pads deposited on the substrate. We avoid depositing Al over the the edges of the membrane to minimize possible mechanical losses at the clamping points.²³ The motion of the membrane is coupled to the cavity field via the antenna. The membrane is anchored on the substrate with $\sim 0.1 \mu\text{l}$ of Bison ‘5 minute’ 2-part epoxy at one corner of the silicon frame. The membrane-embedded 3D cavity is mounted with the plane of the membrane lying horizontally on top of the antenna chip in a cryo-free dilution refrigerator (BlueFors LD250) in which the temperature is controlled between 14 mK and 800 mK.

We measure the cavity response and mechanical motion using microwave reflectometry as described in previous work.¹⁰ A simplified schematic of the reflection measurement is illustrated in Fig.1(b). Microwave signals are attenuated and sent into the cavity. The reflected

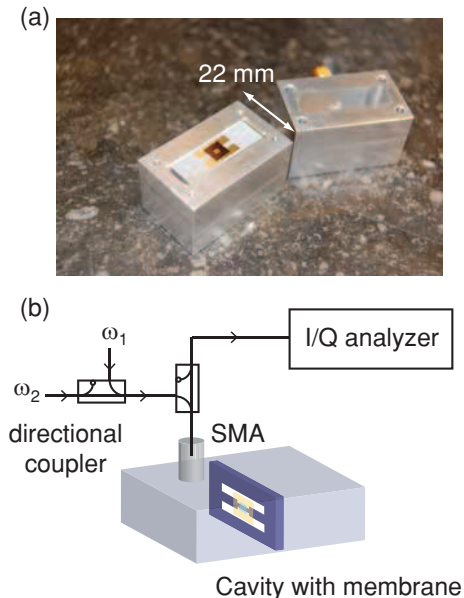


FIG. 1. (a). Photograph of a physical device (Device I), showing two halves of the Al 3D cavity and the membrane resonator. (b). Schematic of the reflection measurement setup. Two microwave tones ω_1 and ω_2 are combined and launched into the membrane-embedded cavity placed inside a dilution refrigerator. The reflected signal is detected by an in-phase/quadrature (I/Q) analyzer. Although the schematic shows the membrane oriented vertically in the illustration, the membrane is mounted horizontally in the fridge.

signal is amplified and read out using a vector signal analyzer (Rohde and Schwarz FSV30) which records the in- and out-of-phase quadrature of the signal V_i and V_q as a function of time within a bandwidth up to 28 MHz around a local oscillator reference frequency. We study two membrane-cavity devices. The cavity resonance ω_0 is $2\pi \times 5.23$ GHz for Device I and $2\pi \times 5.07$ GHz for Device II, with linewidths κ below 300 mK of $2\pi \times 56$ kHz and $2\pi \times 45$ kHz, respectively. The mechanical resonant frequency ω_m and the single-photon coupling rate g_0 for the modes studied are listed in Table I. From the resonant frequency of the fundamental modes, we estimate the effective stress of the metalized membranes to be 0.79 GPa for Device I and 0.09 GPa for Device II, taking an effective density of 3.0 g/cm³. In Device II, the gap to the antenna is 3 μm . In Device I, the gap is 10 μm , resulting in a significantly reduced g_0 .

To measure the quality factor, we drive the membrane at its resonance frequency and then detect the timescale it takes for the motion to ring down (decay). The membrane is driven optomechanically, with a scheme based on an optomechanically-induced transparency (OMIT) measurement.²⁴ As illustrated in Fig. 2(a), two phase-locked microwave signals are sent into the cavity: a swap tone at $\omega_1 = \omega_0 - \omega_m$ and a shake tone at $\omega_2 = \omega_0$. In the presence of the swap tone and the shake tone, there is a beating of the cavity field intensity at ω_m , giving an oscillating radiation pressure force that shakes the drum. From the optomechanical interaction, photons at ω_1 are Raman scattered by the membrane resonator and upconverted into the cavity resonance, producing a mechanical sideband at ω_0 that we use to measure the motion. The I/Q analyzer is set to detect the signal at ω_0 with a sample rate of 100 Hz. Fig. 2(b) shows an example of OMIT measurement taken with Device II in the limit of large optomechanical cooperativity $C = \frac{4g_0^2 N}{\kappa\gamma_m} \gg 1$, where $N \sim 750$ is the number of photons in the cavity generated by the swap tone. To avoid backaction of the swap tone on the motion, for the ringdown measurement we operate in a regime where C of the swap tone is sufficiently small and optomechanical damping γ_{om} is negligible ($C \sim 0.03$, $\gamma_{om} \sim 0.03\gamma_m$).

Fig. 2(c) illustrates the protocol of the optomechanical ringdown measurement. The membrane is first driven into motion when ω_1 and ω_2 are both on. The detected signal at ω_0 consists of the directly reflected signal of the shake tone at ω_2 as well as the mechanical sideband generated from the swap tone at ω_1 . At t_0 the shake tone is switched off, while the swap tone ω_1 stays on. When turning off the shake tone, the associated microwave field at ω_0 decays on a timescale corresponding to κ^{-1} . In addition to the microwave field from the

TABLE I. Summary of mechanical modes studied

Device	I	II		
Mode	(1,1)	(1,1)	(1,2)	(2,1)
$\omega_m/2\pi$ (kHz)	242	121	193	192
$g_0/2\pi$ (Hz)	0.03	0.22	0.01	0.01

shake tone, there is a second microwave field at ω_0 that arises from a sideband of the swap tone generated by the mechanical motion. This second microwave field decays with a much slower timescale corresponding to γ_m^{-1} . On the I/Q analyzer, we then observe a signal at ω_0 from shake tone ω_2 that falls off at the cavity decay rate κ and the remaining mechanical ringdown signal is read out and used to calculate the mechanical amplitude as it decays.

Fig. 3(a) shows an example of a ringdown trace of the mechanical resonator taken at 14 mK. The y -axis is proportional to $V_i^2 + V_q^2$, representing the square amplitude of the resonator. By fitting the curve to an exponential decay $e^{-\gamma_m t}$, γ_m and the quality factor $Q = \omega_m/\gamma_m$ can be extracted. We vary the cryostat temperature T and record the corresponding ringdown traces. The resultant Q -factor as a function of temperature T for Device I (1,1) mode is plot in a linear scale in Fig. 3(b). As T is decreased from 800 mK to 200 mK, there is a relatively flat plateau in Q , consistent with previous results with an optical detection scheme.¹⁸ As T is further reduced to below 200 mK, Q begins to go up, and continues rising with no indication of saturation down to the base temperature of $T = 14$ mK. The highest value $Q = 1.27 \times 10^8$ corresponds to $\gamma_m = 2\pi \times 1.9$ mHz and a time constant for amplitude of $\tau = 2/\gamma_m = 1.6 \times 10^2$ s.

The slight deviation from a straight line in Fig. 3(a) suggests some weak negative non-linear damping, although the mechanical response of the membrane is still in the linear restoring-force regime. The amplitude unity in Fig. 3(a) corresponds to 0.37 nm. For small amplitudes < 0.037 nm, where the deviation becomes significant, we also performed an additional exponential fit, finding a quality factor $Q = 1.16 \times 10^8$ for the lower amplitude regime. The Duffing critical amplitude is estimated to be 6.3 nm with the formulae in Ref. 25 and 26, significantly above the excitation amplitude used here.

In Fig. 3(c) we plot the Q of Device I (1,1) mode (red), Device II (1,1) mode (blue) and Device II (1,2) mode (green) together in a log scale. Quality factors of all three modes

are above 5×10^6 and show similar behavior, improving with decreasing temperature below 200 mK and leveling off between 200 mK and 800 mK. It is also interesting to note that although the mode temperature saturates at 210 mK for Device I and 180 mK for Device II, Q continues to go up as the cryostat is cooled down to base temperature. The high mode temperature in the experiment is likely related to mechanical vibration noise in the setup, which includes only minimal vibration isolation. The fact that we observe an increasing Q down to temperatures far below the mode temperature suggests that the mechanism limiting the Q -factor is not related to the mode occupation. A likely candidate is a physical property of the material itself, such as surface losses.²² In this case, the physical lattice could be thermalized with the fridge, while the mechanical mode is heated out of equilibrium by the vibrational noise.

In contrast to the other modes, Mode (2,1) of Device II has a much lower $Q = 1.2 \times 10^5$ that is independent of temperature from 14 to 800 mK. Although the (1,2) mode and (2,1) are separated by only 1 kHz in frequency, it is striking that Q -factors are different by orders of magnitude. This large difference in Q could result from the anchoring of the chip at one corner, giving very different clamping losses through the substrate chip for the two modes²⁷. With a splitting of the (1,2) and (2,1) into modes symmetric (S) and antisymmetric (AS) with respect to the anchor point, the AS mode could have a temperature-independent Q limited by radiation into the sapphire substrate, while the S mode would then be limited by a different temperature-dependent mechanism.

In the ringdown experiments performed here with the I/Q analyzer, we are able to determine not only the energy loss rate of the mechanical resonator, but also to characterize the dephasing of its mechanical motion. Applying an FFT to the acquired I/Q data from sufficiently long ringdown time trace, one can reconstruct the spectral content of the mechanical resonance during ringdown, giving access to the spectral linewidth Q -factor.²⁸ To do this, we slightly detune the swap tone $\omega_1 = \omega_0 - \omega_m - \delta$ with $\delta = 2\pi \times 31.9$ mHz and measure the I/Q data for 10^4 seconds. In Fig. 4(a) the I/Q vector plot is shown, the x -axis representing the in-phase quadrature V_i and the y -axis the out-of-phase quadrature V_q . The trace forms a spiral: the decrease of the vector length corresponds to the decay in mechanical amplitude, and the angular frequency of the trajectory in the polar plot is determined by δ . To reconstruct a spectrum from the data, we perform an FFT of the complex vector $V_i + jV_q$, $j = \sqrt{-1}$, shown in Fig. 4(b). A fit to the lineshape gives the spectral $Q = 1.10 \pm 0.05 \times 10^8$,

in agreement, to within the error margin, with the ringdown quality factor 1.14×10^8 extracted from the same dataset, demonstrating that the dephasing is not a significant source of decoherence for these membrane resonators.

In conclusion, we have measured the quality factor of SiN_x membranes at millikelvin temperatures with 3D optomechanical cavities. At the base temperature of 14 mK, Q -factors as high as 1.27×10^8 are observed for a fundamental mode, demonstrating the exceptional performance of SiN_x membranes as mechanical resonators. This high Q is achieved in the presence of an Al coating of the membrane, expanding their potential into electrical and microwave applications. By virtue of this low dissipation, SiN_x membranes could be an attractive test bed for quantum superposition states of massive mechanical objects and other applications in optomechanics.

ACKNOWLEDGMENTS

We thank Vibhor Singh and Simon Gröblacher for useful discussions. We acknowledge support from the Dutch Organization for Fundamental Research on Matter (FOM) and the Netherlands Organization for Scientific Research (NWO) through the Innovative Research Incentives Scheme (VIDI).

REFERENCES

- ¹J. D. Thompson, B. M. Zwickl, A. M. Jayich, F. Marquardt, S. M. Girvin, and J. G. E. Harris, *Nature* **452**, 72 (2008).
- ²G. Anetsberger, O. Arcizet, Q. P. Unterreithmeier, R. Rivière, A. Schliesser, E. M. Weig, J. P. Kotthaus, and T. J. Kippenberg, *Nat. Phys.* **5**, 909 (2009).
- ³M. D. LaHaye, O. Buu, B. Camarota, and K. C. Schwab, *Science* **304**, 74 (2004).
- ⁴A. Naik, O. Buu, M. D. LaHaye, A. D. Armour, A. A. Clerk, M. P. Blencowe, and K. C. Schwab, *Nature* **443**, 193 (2006).
- ⁵J. C. Sankey, C. Yang, B. M. Zwickl, A. M. Jayich, and J. G. E. Harris, *Nat. Phys.* **6**, 707 (2010).
- ⁶T. Rocheleau, T. Ndukum, C. Macklin, J. B. Hertzberg, A. A. Clerk, and K. C. Schwab, *Nature* **463**, 72 (2010).

- ⁷T. P. Purdy, R. W. Peterson, and C. A. Regal, *Science* **339**, 801 (2013).
- ⁸T. P. Purdy, P.-L. Yu, R. W. Peterson, N. S. Kampel, and C. A. Regal, *Phys. Rev. X* **3**, 031012 (2013).
- ⁹H. J. Eerkens, F. M. Buters, M. J. Weaver, B. Pepper, G. Welker, K. Heck, P. Sonin, S. de Man, and D. Bouwmeester, *Opt. Express* **23**, 8014 (2015).
- ¹⁰M. Yuan, V. Singh, Y. M. Blanter, and G. A. Steele, *Nat. Commun.* **6**, 8491 (2015).
- ¹¹T. Bagci, A. Simonsen, S. Schmid, L. G. Villanueva, E. Zeuthen, J. Appel, J. M. Taylor, A. Sørensen, K. Usami, A. Schliesser, and E. S. Polzik, *Nature* **507**, 81 (2014).
- ¹²R. W. Andrews, R. W. Peterson, T. P. Purdy, K. Cicak, R. W. Simmonds, C. A. Regal, and K. W. Lehnert, *Nat. Phys.* **10**, 321 (2014).
- ¹³Q. P. Unterreithmeier, E. M. Weig, and J. P. Kotthaus, *Nature* **458**, 1001 (2009).
- ¹⁴T. Faust, P. Krenn, S. Manus, J. P. Kotthaus, and E. M. Weig, *Nat. Commun.* **3**, 728 (2012).
- ¹⁵K. Y. Fong, W. H. P. Pernice, M. Li, and H. X. Tang, *Appl. Phys. Lett.* **97**, 073112 (2010).
- ¹⁶S. S. Verbridge, J. M. Parpia, R. B. Reichenbach, L. M. Bellan, and H. G. Craighead, *J. Appl. Phys.* **99**, 124304 (2006).
- ¹⁷D. Kleckner, B. Pepper, E. Jeffrey, P. Sonin, S. M. Thon, and D. Bouwmeester, *Opt. Express* **19**, 19708 (2011).
- ¹⁸B. M. Zwickl, W. E. Shanks, A. M. Jayich, C. Yang, A. C. Bleszynski Jayich, J. D. Thompson, and J. G. E. Harris, *Appl. Phys. Lett.* **92**, 103125 (2008).
- ¹⁹V. P. Adiga, B. Ilic, R. A. Barton, I. Wilson-Rae, H. G. Craighead, and J. M. Parpia, *J. Appl. Phys.* **112**, 064323 (2012).
- ²⁰S. Chakram, Y. S. Patil, L. Chang, and M. Vengalattore, *Phys. Rev. Lett.* **112**, 127201 (2014).
- ²¹J. Suh, A. J. Weinstein, and K. C. Schwab, *Appl. Phys. Lett.* **103**, 052604 (2013).
- ²²L. G. Villanueva and S. Schmid, *Phys. Rev. Lett.* **113**, 227201 (2014).
- ²³P.-L. Yu, T. P. Purdy, and C. A. Regal, *Phys. Rev. Lett.* **108**, 083603 (2012).
- ²⁴S. Weis, R. Rivière, S. Deléglise, E. Gavartin, O. Arcizet, A. Schliesser, and T. J. Kippenberg, *Science* **330**, 1520 (2010).
- ²⁵V. A. Chobotov and R. C. Binder, *J. Acoust. Soc. Am.* **36** (1964).
- ²⁶I. Kozinsky, *Nonlinear Nanoelectromechanical Systems*, Ph.D. thesis, California Institute of Technology (2007).

²⁷S. Schmid, K. D. Jensen, K. H. Nielsen, and A. Boisen, Phys. Rev. B **84**, 165307 (2011).

²⁸B. H. Schneider, V. Singh, W. J. Venstra, H. B. Meerwaldt, and G. A. Steele, Nat. Comms. **5**, 5819 (2014).

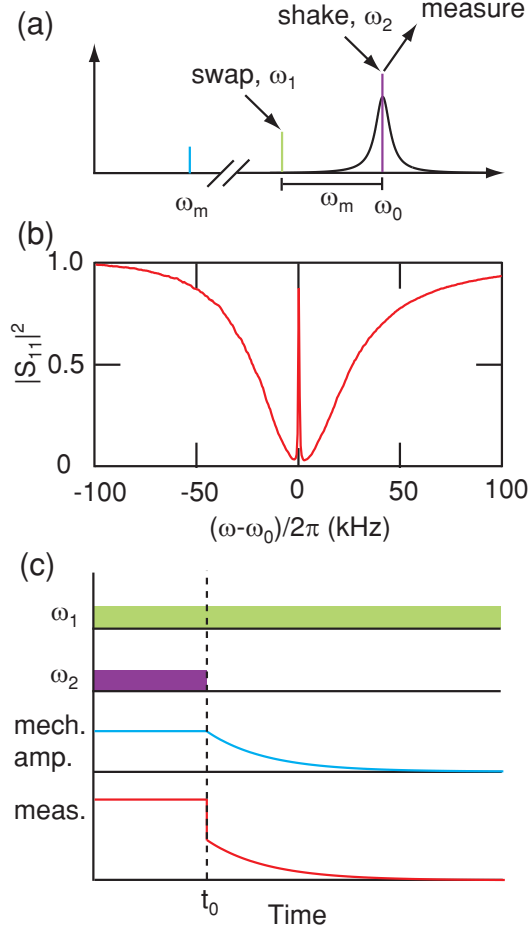


FIG. 2. (a). Schematic of the measurement scheme. A swap tone at ω_1 is used to induce an optomechanical swap interaction between the cavity and the membrane. Another tone at $\omega_2 = \omega_0$ is used to shake the membrane. A vector signal analyzer is used to detect signal at ω_0 . (b). OMIT with $C \gg 1$, showing $|S_{11}|^2$ as a function of frequency. To avoid optomechanical backaction, ringdown measurement is carried out in the $C \ll 1$ regime. (c) Schematic for measurement of ringdown with OMIT configuration. The swap tone ω_1 is kept on at all time while the shake tone is switched off at t_0 , at which point the mechanical resonator starts to decay. The signal measured at ω_0 is a sum of the mechanical sideband generated by ω_1 and the reflected signal generated by ω_2 . When ω_2 is switched off, the latter decays at a rate of κ , and the remaining mechanical component of the signal at ω_2 then rings down on a time scale corresponding to γ_m^{-1} .

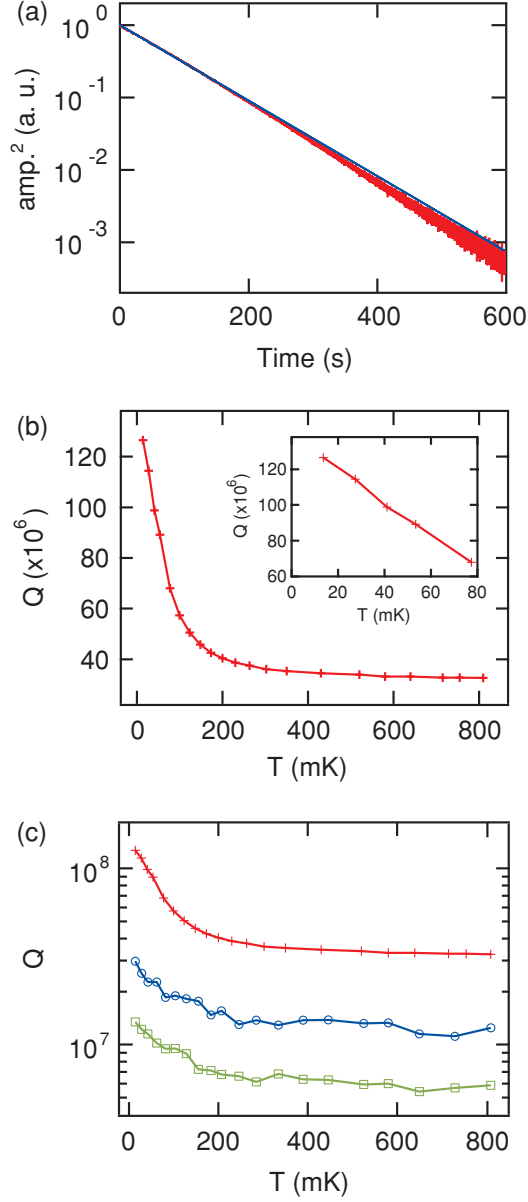


FIG. 3. (a). Time trace of the mechanical amplitude during ringdown for Device I at 14 mK. From a fit to exponential decay, we extract the mechanical quality factor. Red: data; blue: fit. The deviation from a straight line may indicate some weak negative nonlinear damping. (b). Extracted quality factor Q of the membrane resonator as a function of cryostat temperature for Device I (1,1) mode. Inset: zoom-in for $T < 80$ mK. The highest value is $Q = 1.27 \times 10^8$ for Device I at 14 mK. (c). Extracted quality factor for both samples. Red: Device I (1,1) mode; blue: Device II (1,1) mode; green: Device II (1,2) mode. Q decreases with increasing temperature for $14 \text{ mK} < T < 200 \text{ mK}$, leveling out between 200 mK and 800 mK.

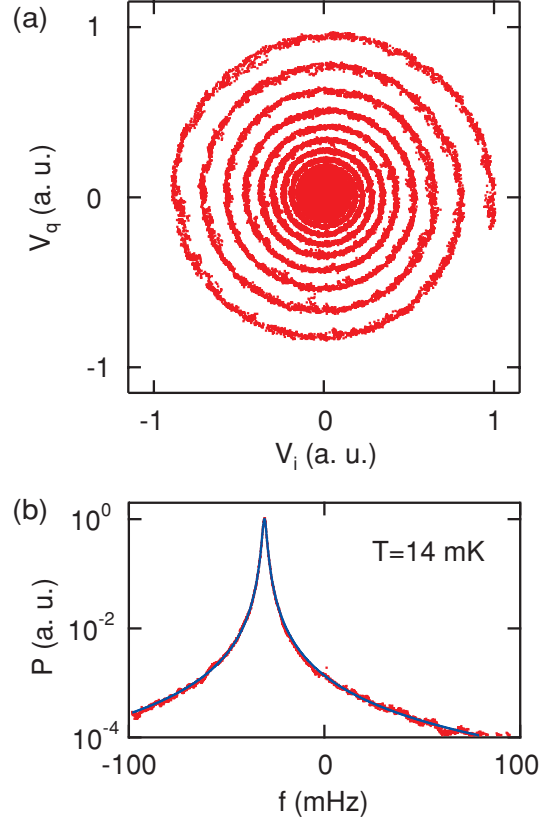


FIG. 4. I/Q analysis of the ringdown trace. Swap tone is set to $\omega_1 = \omega_0 - \omega_m - \delta$, $\delta = 2\pi \times 31.9$ mHz. (a). Out-of-phase quadrature V_q vs. in-phase quadrature V_i . Decay of the amplitude in combination with the detuning δ of the swap tone results in a spiral that circles around the origin at an angular frequency δ . (b). FFT spectrum of the complex temporal I/Q trace. Red: data; blue: fit. From the linewidth of the resonance the decoherence, including dephasing and relaxation, can be extracted. By comparing the spectral quality factor $1.10 \pm 0.05 \times 10^8$ and the ringdown quality factor 1.14×10^8 , the contribution of dephasing to the spectral linewidth is negligible within the error margin.